Available online at www.sciencedirect.com

jmr&t Journal of Materials Research and Technology

journal homepage: www.elsevier.com/locate/jmrt

Revealing microstructural evolutions, mechanical properties and wear performance of wire arc additive manufacturing homogeneous and heterogeneous NiTi alloy

J.Z. Teng [a,1], P.F. Jiang [a,b,1], X.H. Cui [a], M.H. Nie [a,b], X.R. Li [a,b], C.Z. Liu [c], Z.H. Zhang [a,b,*]

[a] Key Laboratory of Bionic Engineering, (Ministry of Education), College of Biological and Agricultural Engineering, Jilin University, 5988 Renmin Street, Changchun 130025, PR China

[b] Institute of Structured and Architected Materials, Liaoning Academy of Materials, Shenyang 110167, China

[c] Institute of Orthopaedic & Musculoskeletal Science, University College London, Royal National Orthopaedic Hospital, Stanmore, London HA7 4LP, UK

ARTICLE INFO

Article history:
Received 7 September 2023
Accepted 5 October 2023
Available online 9 October 2023

Keywords:
NiTi alloy
Wire arc additive manufacturing
Microstructure
Mechanical properties
Wear performance

ABSTRACT

Heterogeneous microstructure designs have attracted a great deal of attention, not only because they have the potential to achieve an ideal combination of two conflicting properties, but also because the processes involved in their fabrication are cost-effective and can be scaled up for industrial production. The process parameters in the preparation process have an important effect on the microstructure and properties of alloy members prepared by wire arc additive manufacturing (WAAM) technology. It was expected that the spatial heterogeneous microstructure with large microstructural heterogeneities in metals can be formed through changing the process parameters. In this work, homogeneous NiTi thin-walled component and heterogeneous NiTi thin-walled component were fabricated using WAAM technology by adjusting the heat input. The effects of deposition height and heat input on the microstructure, mechanical properties and wear properties of WAAM NiTi alloys were investigated. The results show that grains were gradually refined with the increase of deposition height in the homogeneous WAAM NiTi component. The ultimate tensile strength of homogeneous WAAM NiTi component increased from 606.87 MPa to 654.45 MPa and the elongation increased from 12.72% to 15.38%, as the increase of deposition height. Moreover, the homogeneous WAAM NiTi component exhibited excellent wear resistance, the coefficient of friction decreased from 0.760 to 0.715 with the increase of deposition height. Meanwhile, the grains in the heterogeneous WAAM NiTi component shows the finest grains in the central region. The ultimate tensile strength of the lower region, middle region and upper region of heterogeneous WAAM NiTi components were 556.12 MPa, 599.53 MPa and 739.79 MPa, and the elongations were 12.98%, 16.69%, 21.74%, respectively. The coefficient of friction for the lower region, middle region and upper region of heterogeneous WAAM NiTi components were 0.713, 0.720 and 0.710, respectively. The microhardness and cyclic compression properties of the homogeneous components with

* Corresponding author. Key Laboratory of Bionic Engineering, (Ministry of Education), College of Biological and Agricultural Engineering, Jilin University, 5988 Renmin Street, Changchun 130025, PR China.
E-mail address: zhzh@jlu.edu.cn (Z.H. Zhang).

[1] These authors contributed equally to this work.

https://doi.org/10.1016/j.jmrt.2023.10.055

higher heat input were better than those of the heterogeneous components for the same deposition height. The tensile yield strength, elongation and wear resistance of the heterogeneous components were superior compared to the homogeneous components. These results can be used to optimize the WAAM process parameters to prepare NiTi components with excellent mechanical properties.

1. Introduction

NiTi alloys have a wide range of applications in medical devices, aerospace and marine development due to its unique superelasticity, good shape memory, excellent biocompatibility and corrosion resistance [1]. Due to their superelasticity, these alloys can produce large deformations under external forces, however, return to their authentic form after releasing the exterior load. On the other hand, NiTi alloys with shape memory properties can completely return to the original shape before deformation when heated to a certain temperature after a certain plastic deformation under some conditions [2,3]. The traditional processing methods of NiTi alloy mainly include powder metallurgy and traditional melting method. However, NiTi alloys are difficult to machine owing to their high hardness, adhesion and rebound response. Therefore, it is particularly important to develop NiTi alloy manufacturing technology with low cost, high efficiency and high production accuracy [4,5].

Additive manufacturing technologies can be categorized according to the heat source into laser additive manufacturing (LAM), electron beam additive manufacturing (EBAM), and wire arc additive manufacturing (WAAM) [6]. According to the way the powder is given, LAM technology can be categorized into two types powder spreading and powder feeding. Although the application of laser additive manufacturing technology is more extensive, limited by the molding size, equipment price, powder cost, molding efficiency and other factors, is not suitable for molding large structural components. Electron beam additive manufacturing processing conditions are vacuum environments, which help to control the impurity content of the component, but also limit the volume of the processed components [7]. WAAM is getting more and more attention from researchers at home and abroad due to that it has high heat input and high molding efficiency and is suitable for large-size complex components. Moreover, WAAM has low equipment costs and high material utilization. It has the incomparable efficiency and cost advantages of other additive technologies [8,9]. Therefore, WAAM has a huge advantage over other additive manufacturing methods to obtain higher productivity of NiTi alloy components [10,11].

Most studies on AM NiTi have focused on material property optimization, studying the evolution of microstructure, phase transition and mechanical response of NiTi alloys under different conditions [12,13]. It should be pointed out that in the WAAM process, different process parameters will lead to different heat input, which will affect the change of microstructure and mechanical properties at different deposition heights. Moreover, the process parameters also have a great influence on the martensitic phase transition behavior of NiTi alloys because the martensitic phase transition behavior of NiTi alloys is affected by many factors, including material composition, heat treatment conditions during processing and external stresses. Therefore, it is necessary to control the WAAM process parameters, since variations in the parameters will lead to variations in the martensitic phase transition temperature of NiTi alloys, which in turn will affect the microstructure and properties of the NiTi components produced [14]. It is well known that a higher heat input will result in a lower cooling rate and a longer solidification time, resulting in coarse grains [15,16]. Therefore, the grain size, grain boundary state and chemical composition of NiTi alloy can be adjusted by controlling the heat input conditions of molten pool, which can affect the phase transformation behavior and mechanical properties of the alloy.

However, through a large number of literature studies, it was found that many studies have focused on the effect of changes in deposition height and peak current intensity on the change in properties of WAAM NiTi alloys. The thermal input of molten pool energy serves as one of the most important process parameters in the additive manufacturing process. It is proportional to voltage and current and inversely proportional to travel speed [17]. Wang et al. [18] researched the effects of substrate heating temperature on the phase transformation and mechanical performance of NiTi during the WAAM process. Their study found that the phase transition temperature increased as the substrate heating temperature increased, suggesting that the martensitic phase transition was prone to occur. They suggested that the variation of the functional properties of NiTi alloy with the heating temperature of the matrix could be attributed to the effect of grain refinement and precipitation hardening, as well as the [100] texture strength. They also reported that the effect of the deposition current on crystallographic orientation and mechanical performance of dual-wire arc additive manufactured Ni-rich NiTi alloy [19]. The results showed that with the increase of deposition current, the texture strength decreased gradually, the size of precipitated phase of Ni_4Ti_3 increased generally, and the characteristic phase transition temperature increased. Moreover, the tensile results revealed that for increasing deposition current from 80 A to 100 A, the ultimate tensile stress was lowered from 927.9 to 613.8 MPa and elongation was reduced from 8.7 to 5.6%. Pu et al. [20]

studied the microstructure, phase transformation behavior and tensile superelasticity of the wire-based vacuum additive manufacturing NiTi alloy. They found that the deposition height affected the microstructure, phase transition behavior and tensile superelasticity of NiTi alloys. The resulted showed that the grain size increased gradually from bottom to top due to epitaxial grain growth with a single heat dissipation direction and a slow cooling rate. In addition, the top region of the alloy member showed better superelasticity. Wang et al. [21] investigated the effect of linear heat input on the microstructure and mechanical properties of AM 304L. Their study found a link between linear heat input, grain size and yield strength in AM. The yield strength, ultimate tensile strength, and ductility were higher for the low linear heat input wall compared to the high linear heat input wall. The microstructure was coarser at the top compared to the bottom. Based on the above discussion, it is noticed that the studies on effect of process parameters on homogeneous alloy components are already available in the literature. No previous publication has demonstrated the effect of process parameters on heterogeneous NiTi alloy components manufactured by WAAM technology. Therefore, it is necessary to investigate the effects of process parameters on the microstructure and properties of heterogeneous NiTi alloy components.

In this study, thin-walled components of homogeneous and heterogeneous NiTi alloys were prepared by using the WAAM technique at the same peak current (220 A) and different peak currents (200 A-210 A-220 A), respectively. The effect of different heat inputs on microstructure evolution, phase transformation, mechanical properties and wear performance in the WAAM process were carried out. The theoretical and experimental basis was provided for the process design and controlled organization and performance of WAAM NiTi alloys. The implementation of this project can provide a theoretical basis for optimizing WAAM technology to prepare NiTi components.

2. Materials and methods

2.1. WAAM system and material

The NiTi components were fabricated using the established WAAM system, which consists of a six-axis ABB robotic arm, an inert gas module, a wire feed system and other basic elements of the WAAM. This WAAM system had been introduced in further detail in other articles [9,10]. The WAAM device schematic diagram is shown in Fig. 1. A tungsten inert gas (TIG) torch was mounted on the six-axis robotic arm that can move flexibly in space. The environment for deposition is an inert gas-protected environment filled with 99.99% high-purity argon gas. A NiTi alloy substrate with a size of 150 mm × 150 mm × 10 mm was used as the substrate.

NiTi welding wire with diameter of 1.2 mm was used as raw material. The element distribution of the welding wire is (wt%): 55.85 Ni, 0.039 O, 0.032 C, 0.025 Nb and balance Ti. The XRD and DSC results of the NiTi wire are shown in Fig. 2. In the XRD results, only a distinct austenitic phase was observed, proving that it did not undergo martensitic phase transformation at room temperature conditions, as shown in Fig. 2(a). In the DSC results, the presence of only one phase transition peak during both heating and cooling indicated that the phase transition experienced by the NiTi filaments was reversible and no non-reversible phase transition or phase transition overlap occurred, as shown in Fig. 2(b). On the basis of the earlier basic studies, the optimized two sets of experimental parameters were set, and the parameters are shown in Table 1. Schematic diagram of the deposition components of the two components is shown in Fig. 3. The pre-component was separated from the NiTi substrate by a wire electrode cutter and the required component was cut according to Fig. 4(a). Without post-processing heat treatment, square components of 10 mm × 10 mm × 10 mm dimensions were cut from different deposition heights of the built-up components

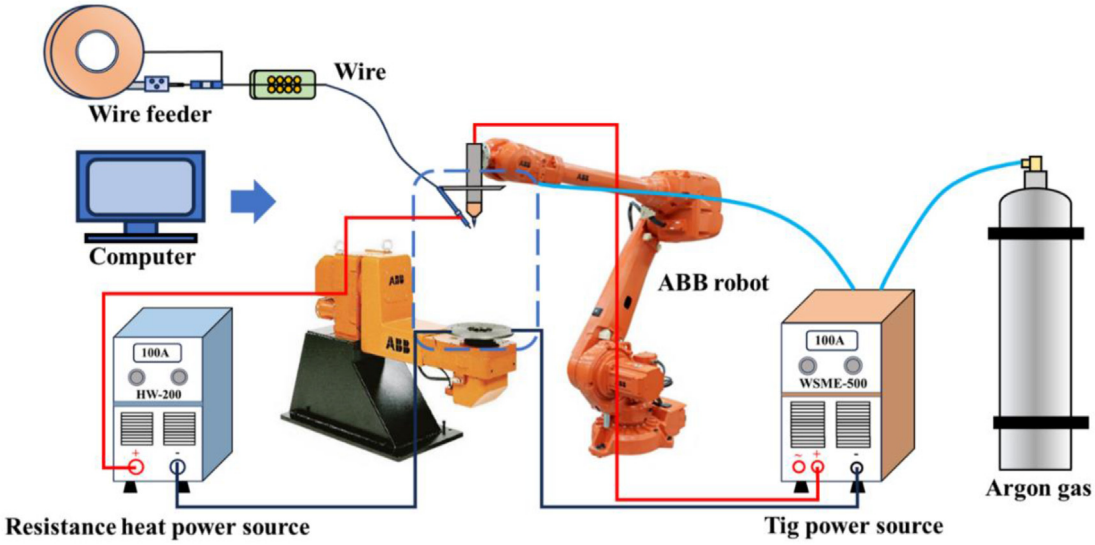

Fig. 1 – Schematic of the WAAM system.

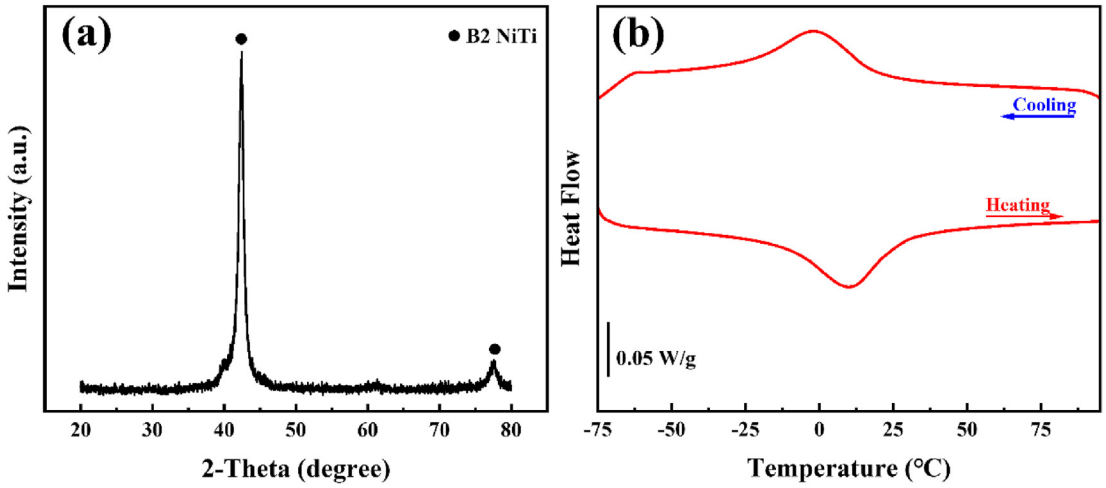

Fig. 2 – Characterization of the NiTi wire: (a) XRD; (b) DSC.

and differentiated into upper, middle, and lower components. The dimension of the component is shown in Fig. 4(b).

2.2. *Characterization*

To remove the effects of surface treatment, the component surfaces were ground by 60#-2000# SiC sandpaper and polished with 2.5 μm and 1 μm diamond paste. In order to investigate the surface microstructure, the WAAM components were etched with a solution (1 ml of HF, 6 mL of HNO_3 and 100 ml of H_2O) for 10 s. The microstructure of the components was characterized by optical microscopy (OM) and field emission scanning electron microscopy (SEM). The phase composition of the samples was determined using X-ray diffraction (XRD). The diffraction angle set to 20°–80° and the scanning speed set to 4°/min.

The microhardness of NiTi component sections was determined using a Vickers automated hardness tester (Huayin, HVS-1000). The loading load was 200 g, and the dwell time was 15 s.

The phase transition behavior was qualified by differential scanning calorimetry (DSC, Discovery DSC 25) with a cooling/heating speed of 10°/minute and a variation interval of −80°–100°.

The tensile property was performed at room temperature using the tensile system (Instron 1121 tester), with a loading rate of 0.5 mm/min. The dimension of the tensile sample is shown in Fig. 4(c). The fracture morphology was analyzed using scanning electron microscopy (SEM).

The compression tests were performed at room temperature with the compression tester. The loading rate of the compression fracture test was 0.5 mm/min, and the loading rate of the cyclic compression test was 0.5 mm/min. The compression sample size was Φ 4 mm × 8 mm. The dimension of the compression sample is shown in Fig. 4(d).

Low speed friction experiments on NiTi samples were carried out using a (UMT-5, Bruker) friction tester. The friction time was set to be 30 min, friction speed to be 5 mm/s and friction load to be 20 N. The morphology of the wear marks was analyzed using scanning electron microscopy (SEM).

3. Results and discussion

3.1. *Optical microscopy*

Fig. 5 shows the photomicrographs of WAAM homogeneous NiTi thin walls prepared with constant heat input and heterogeneous NiTi thin walls prepared with varying heat input at different deposition heights. In the upper, middle and lower regions of both thin-walled components, there were obvious columnar organizations observed. In contrast, the lower columnar crystals were coarser, as shown in Fig. 5. The upper columnar crystals were finer and had a tendency to shift towards equiaxial crystals. In comparison, the columnar crystals of the heterogeneous elements with the same deposition height were coarser. The thermal gradient generated was more pronounced due to the change in thermal input of the heterogeneous components under the middle and lower portions, which resulted in coarser grains. No significant pores or cracks were observed in any of the regions. The microstructural morphology exhibited at different deposition heights of

Table 1 – The optimized WAAM process parameters about this experiment.

Region		Peak current (A)	Base current (A)	NiTi wire feed velocity (cm/min)	NiTi hot-wire current (A)	Moving speed (mm/min)	Shielding gas flow rate (L/min)
Homogenous		220	9	80	100	300	20
	Lower Region	200	9	80	100	300	20
Heterogeneous	Middle Region	210	9	80	100	300	20
	Upper Region	220	9	80	100	300	20

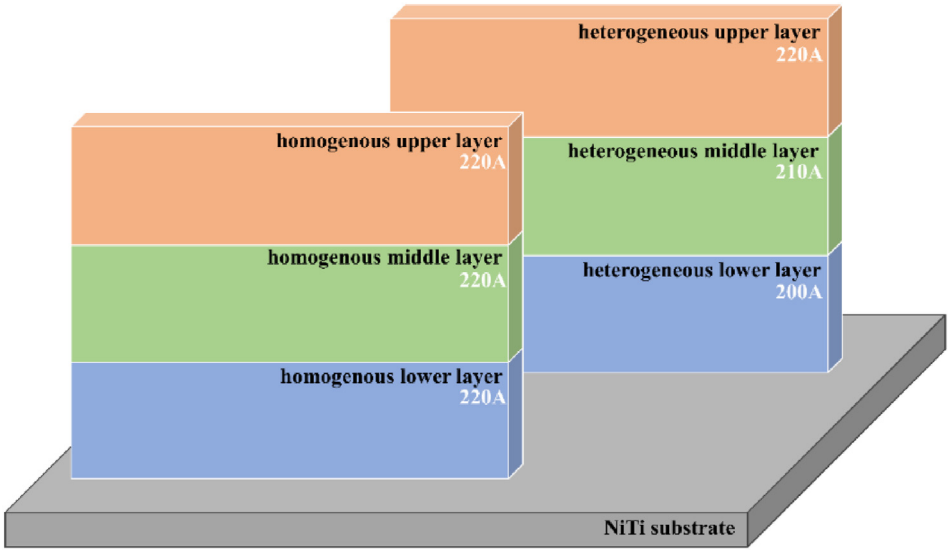

Fig. 3 – Schematic diagram of WAAM fabrication NiTi homogeneous and heterogeneous alloys.

NiTi walls was greatly influenced by the behavior of the ongoing remelting thermal cycling during the deposition of NiTi alloys. Therefore, there were different thermal gradients and grain growth rates in different regions. In the initial stage of NiTi alloy deposition by WAAM, the heat generated by the deposition process is mainly conducted along the substrate plane, thus creating a large thermal gradient. As a result, a columnar grain structure appeared in the lower region of the components. Due to the cyclic heating and remelting of the subsequent deposition process, the columnar crystal structure grew by extension from the lower to the higher region of the deposition height [22]. Therefore, the microstructure in

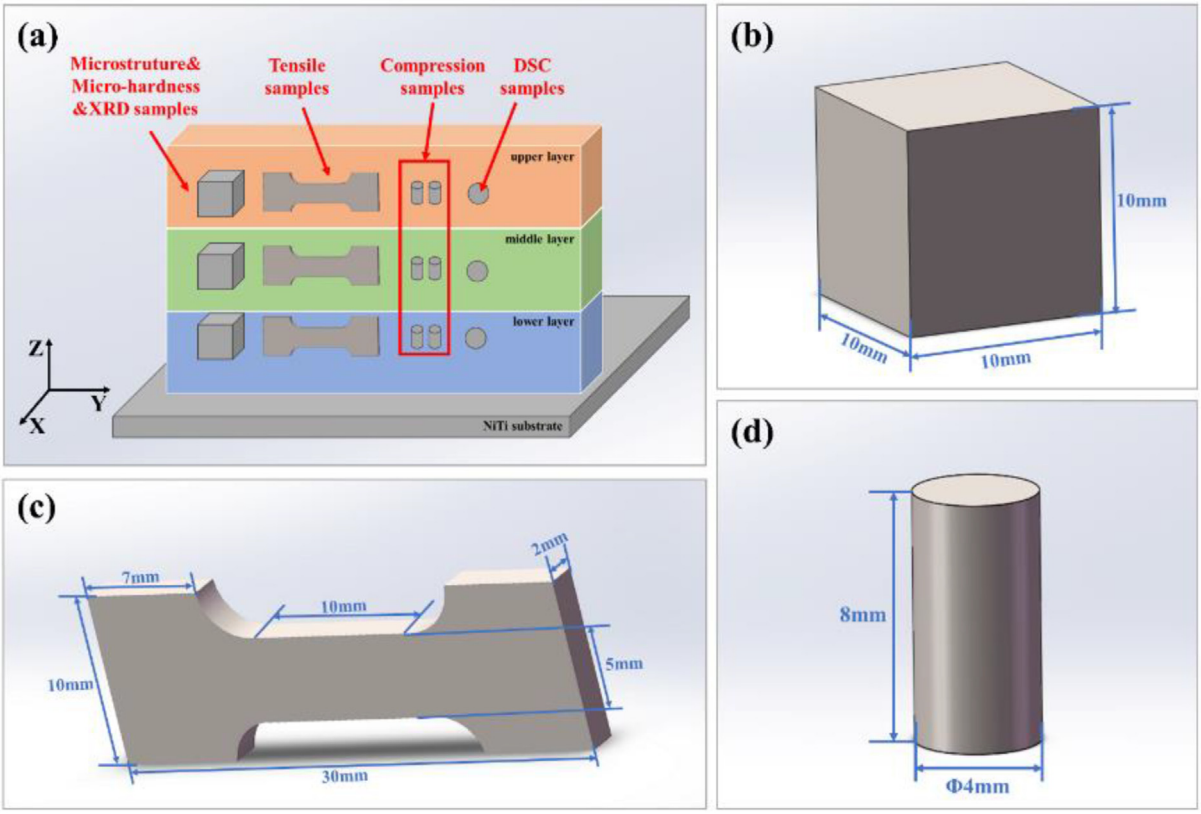

Fig. 4 – (a) Sample preparation for microanalysis, microhardness, XRD, DSC, tensile and compression tests; (b) Size of block sample; (c) Size of tensile test sample; (d) Size of compression test sample.

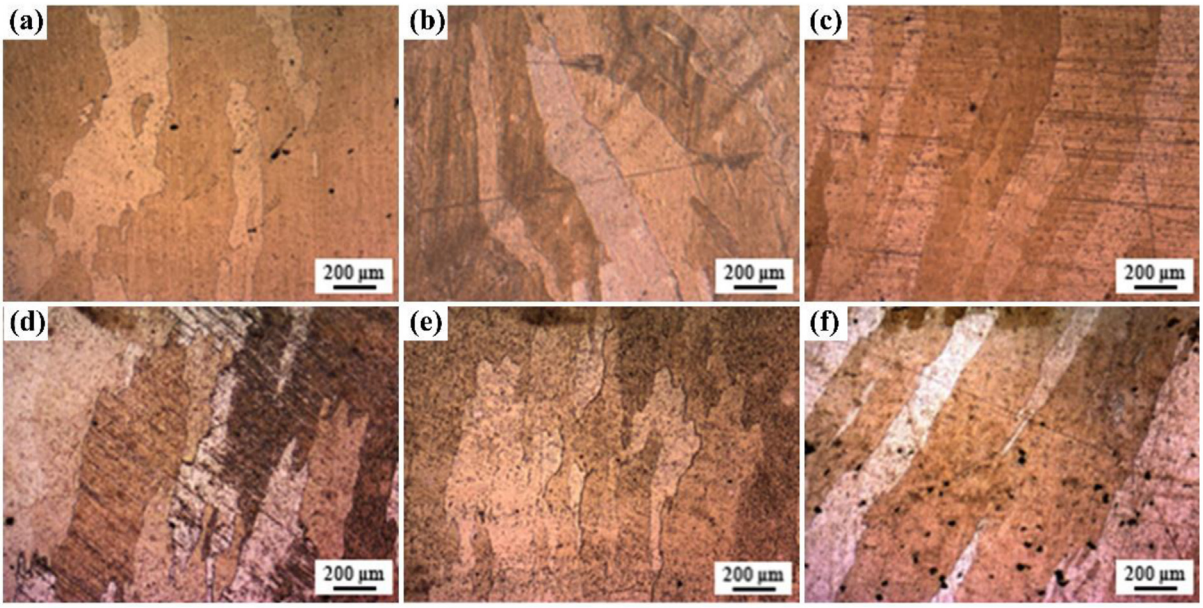

Fig. 5 – OM images (Y-Z plane) of the upper, middle, and lower regions of WAAM fabricated NiTi walls: (a)–(c) homogeneous NiTi wall; (d)–(f) heterogeneous NiTi wall.

the cross section of the WAAM NiTi component was predominantly columnar crystal structure and was coarsest in the lower region.

In addition, the continuous cyclic back-and-forth motion of the molten droplets along the path during the deposition process leaded to a change in the direction of heat transfer within the component, resulting in the formation of columnar grains with unsmooth grain boundaries. In the middle region of the two components, the size of the columnar grain was smaller than that in the lower region, which may be due to the reduced number of thermal cycles experienced during subsequent deposition. Since the number of thermal cycles experienced in the last layers of deposition was reduced, the cooling rate was accelerated, resulting in the formation of a small columnar structure in the upper region [23]. Unlike the homogeneous component, the columnar crystals in the middle region were finer than the upper region in the heterogeneous component, as shown in Fig. 5(d)–(e). Due to the higher preheating temperature and higher thermal cycling temperature in the upper region of the heterogeneous component, the columnar crystals in the upper region were coarser.

3.2. *XRD analysis*

XRD characterization tests were performed at room temperature and the phase composition of the resulting NiTi samples is shown in Fig. 6. The main composition of the homogeneous samples was B2 austenite phase in all regions of different deposition heights. In addition, Ni_4Ti_3 intermetallic phase was also detected in the upper region. The presence of additional phases was not detected in all regions of the homogeneous component. With the increase of deposition height, the martensitic phase (B19′) appeared and expanded. Only in the upper region, secondary phases such as Ni_4Ti_3 can be observed. When the samples underwent a sufficient number of thermal cycles in the lower and middle regions, it allowed the decomposition of metastable Ni_4Ti_3 into stable Ni_3Ti precipitation [24]. However, the presence of the Ni_4Ti_3 phase was only observed in the upper region because it did not undergo repeated remelting conditions. In addition, in the heterogeneous NiTi thin wall with altered heat input, only B2 austenite phase was present in all three regions, as shown in Fig. 6(b). The metastable Ni_4Ti_3 in the upper region can decomposed into stable Ni_3Ti precipitates in a short time due to the heat input increased with the increase of deposition height. Previous studies have shown that Ni_4Ti_3 can provide significant strengthening of samples. Therefore, the upper region of the homogeneous sample may exhibit better properties than the rest of the region [25].

3.3. *Microstructure analysis*

SEM images of the different deposition height regions of the homogeneous NiTi walls and heterogeneous NiTi walls prepared by WAAM are shown in Fig. 7. The composition of the matrix phases and precipitated phases at different locations as determined by the spectrometer is shown in Table 2. In the upper region of the homogeneous component, the precipitated phases distributed sparsely, and the morphology is mainly point-like, as shown in Fig. 7(a). There are obvious martensitic fine crystals in the lower and middle regions of the homogeneous NiTi wall, and point-like precipitated phases disperse on the matrix, as shown in Fig. 7(b) and (c). Significant point-like precipitated phases are also seen at the lower region of the heterogeneous NiTi component. However, the linear precipitated phases are more diffuse at the middle region of the heterogeneous NiTi wall that is illustrated in Fig. 7(e). According to the results of EDS, it can be found that most of the precipitated phases were $NiTi_2$ phase.

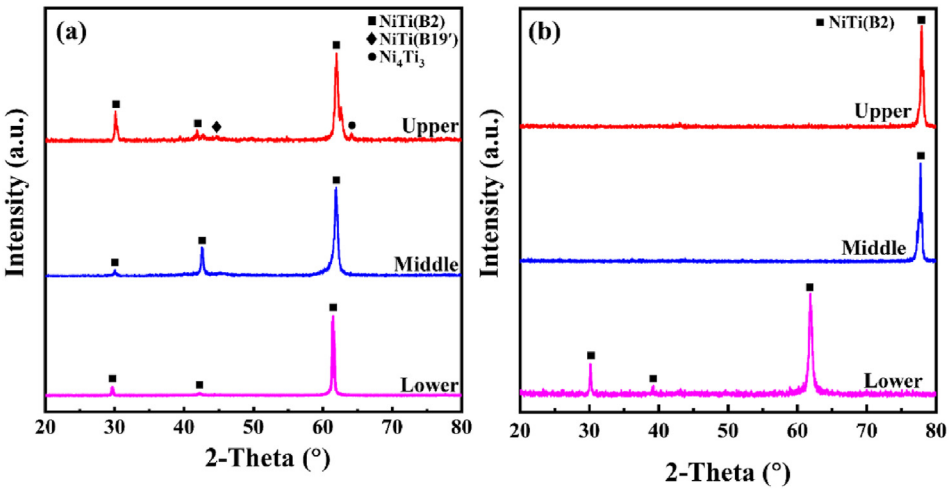

Fig. 6 – XRD patterns of samples in the upper, middle and lower regions of NiTi walls: (a) homogeneous NiTi wall; (b) heterogeneous NiTi wall.

Wang et al. [26] found that the content of secondary phase precipitates differed significantly at different deposition heights of the NiTi thin wall. Differences in the content of secondary term precipitates in NiTi alloys lead to differences in the content of Ni in the matrix, while the content of Ni in NiTi alloys affects the mechanical properties of the samples [27]. In contrast, for the present work, the precipitated phases were mostly $NiTi_2$ phases at the different deposition height. This was mainly due to the intrinsic advantages of the WAAM process (good thermal management), which resulted in that the WAAM-prepared NiTi walls have uniform distribution of Ni content and Ti content in the direction of deposition height.

3.4. *Microhardness distribution*

The microhardness evolution of homogeneous and heterogeneous NiTi walls along the build direction were characterized in Fig. 8. The hardness distribution pattern of both homogeneous and heterogeneous NiTi alloy components showed that the microhardness first decreased and then increased as the deposition height went from low to high. The microhardness is lowest in the middle region and highest in the upper region. The average hardness of the homogeneous NiTi alloy samples in the lower, middle and upper regions were around 270HV, 239.5HV, and 339.6HV, respectively. The average hardness of the heterogeneous NiTi alloy samples in

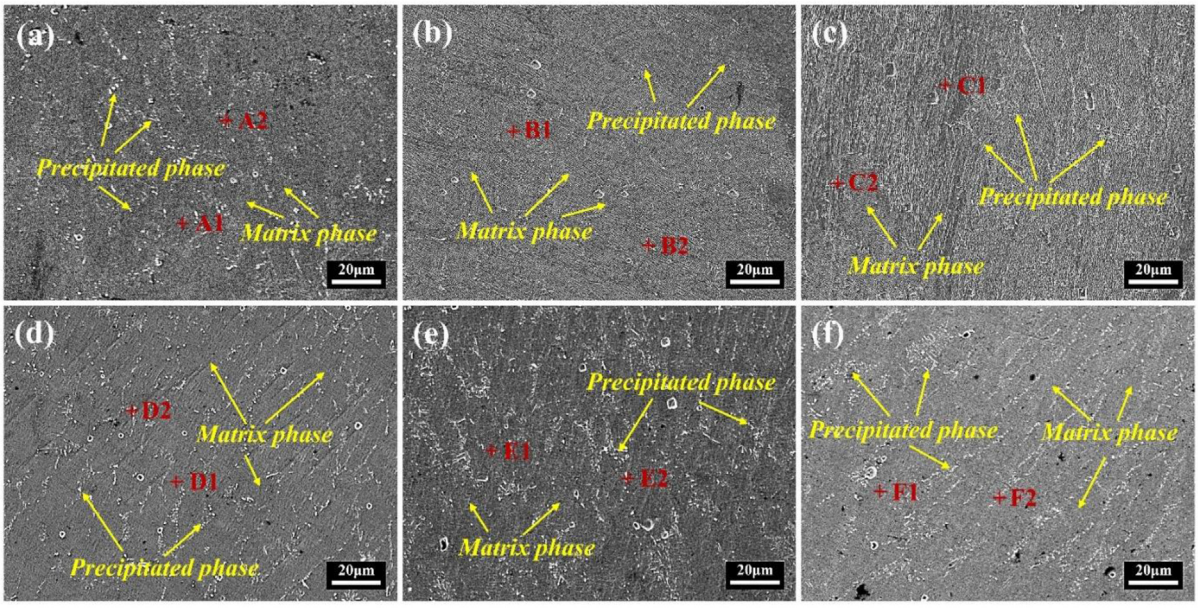

Fig. 7 – SEM images (Y-Z plane) of the upper, middle, and lower regions of WAAM fabricated NiTi walls: (a)–(c) homogeneous upper, middle and lower sections; (d)–(f) heterogeneous upper, middle and lower parts.

Table 2 – EDS results of chemical compositions at each area marked in Fig. 7.

Positions	Ni content (at%)	Ti content (at%)	Suggested phases
A1	50.63	49.37	Matrix (NiTi)
A2	28.75	71.25	$NiTi_2$
B1	50.04	49.96	Matrix (NiTi)
B2	38.12	61.88	$NiTi_2$
C1	49.44	50.56	Matrix (NiTi)
C2	48.66	51.34	NiTi
D1	50.20	49.80	Matrix (NiTi)
C2	37.26	62.74	$NiTi_2$
E1	49.77	50.23	Matrix (NiTi)
E2	39.83	60.17	$NiTi_2$
F1	49.62	50.38	Matrix (NiTi)
F2	30.22	69.78	$NiTi_2$

the lower, middle and upper regions were around 255.2HV, 235.4HV, and 303.2HV, respectively. The average hardness of heterogeneous NiTi alloy sample had smaller fluctuations than that of the homogeneous alloy sample. The variation of columnar grain size and secondary phase precipitate content with deposition height leaded to the microhardness distribution pattern described above. The increased number of grain boundaries in fine grains, coupled with the fact that crystal defected in fine grains were more likely to restrict the movement of dislocations, results in an increase in the hardness of materials with fine grains [28]. As the deposition height increased, the size of the columnar crystals decreased, so the microhardness of the upper region with the smallest columnar crystals should be the greatest. The presence of Ni_4Ti_3 phase can improve the microhardness of NiTi matrix [29]. For a combination of these reasons, the upper regions of both homogeneous and heterogeneous NiTi alloy samples exhibit the highest stiffness. On the other hand, the frequent thermal cycling of the lower region leaded to an increase in its microhardness. As a result, the microhardness of the lower region will be slightly higher than that of the middle region. According to the above reasons, the microhardness of the upper region is the highest and the microhardness of the middle region is the lowest in both homogeneous and heterogeneous NiTi alloy samples.

3.5. *Phase transformation behavior*

The phase transition behavior of NiTi homogeneous and heterogeneous NiTi alloy components with different deposition heights was analyzed by DSC tests, and the experimental outcomes are illustrated in Fig. 9. The results (Table 3) showed that: The phase transition temperature of the NiTi alloy samples failed to reach room temperature, owing to which the austenitic B2 phase was formed. The middle and lower regions of the homogeneous NiTi alloy sample both showed two peaks during the cooling process, as shown in Fig. 9(a). The B2 phase of NiTi alloys can transform to the R phase and the B19′ phase during the cooling process, and the conditions of the transformation are related to their respective free energies. During the cooling process, the free energy of the B19′ phase and the free energy of the B2 phase will change. The B2–B19′ transition occurred when the free energy of the B19′ phase was lower than that of the B2 phase, while the B2-R transition occurred first when the free energy of the R phase was lower than the B2 phase and B19′ phase. Hence two peaks appeared indicating a B2-R-B19 transition in the homogeneous NiTi alloy samples. The temperature difference between the R_S in the lower region and the M_S in the upper region of the homogeneous NiTi alloy component was in a small range, as illustrated in Fig. 9(b). The initial phase transition temperature of the homogeneous NiTi alloy component prepared by WAAM process was the highest in the middle region. In the heterogeneous NiTi alloy components, only one peak was present in all three regions at different deposition heights. Meanwhile, the phase transition peak gradually shifted to the left and the height of the phase transition peak decreased with the increase in deposition height, as shown in Fig. 9(c). The M_S of the heterogeneous NiTi alloy component increased gradually with the height of deposition, as shown in Fig. 9(d). It was well accepted that the Ni content affects the phase transition behavior of the NiTi alloy, and a decrease in the Ni content will cause a significant increase in the Ms temperature [30]. With

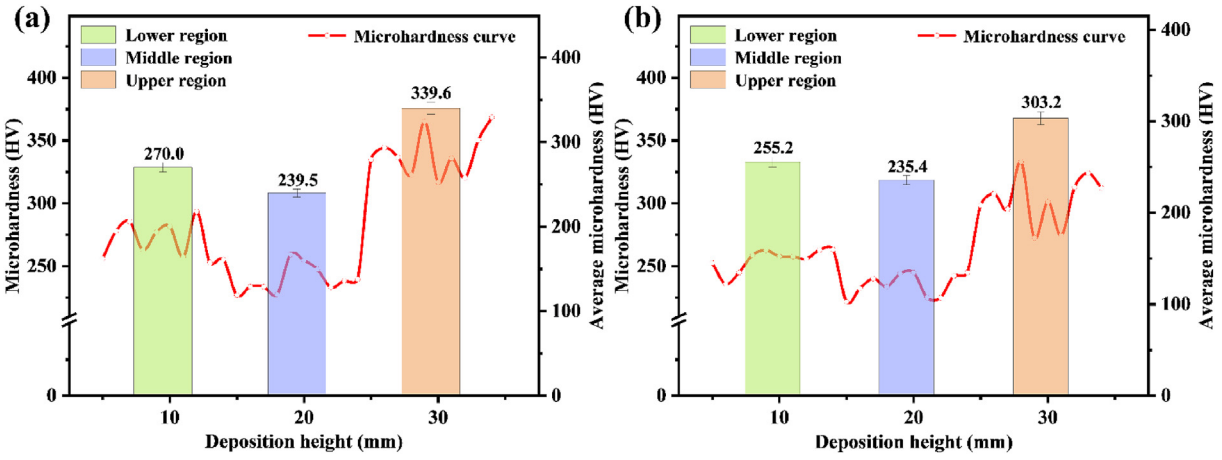

Fig. 8 – Evolution of microhardness with changing deposition height of NiTi walls: (a) homogeneous NiTi wall; (b) heterogeneous NiTi wall.

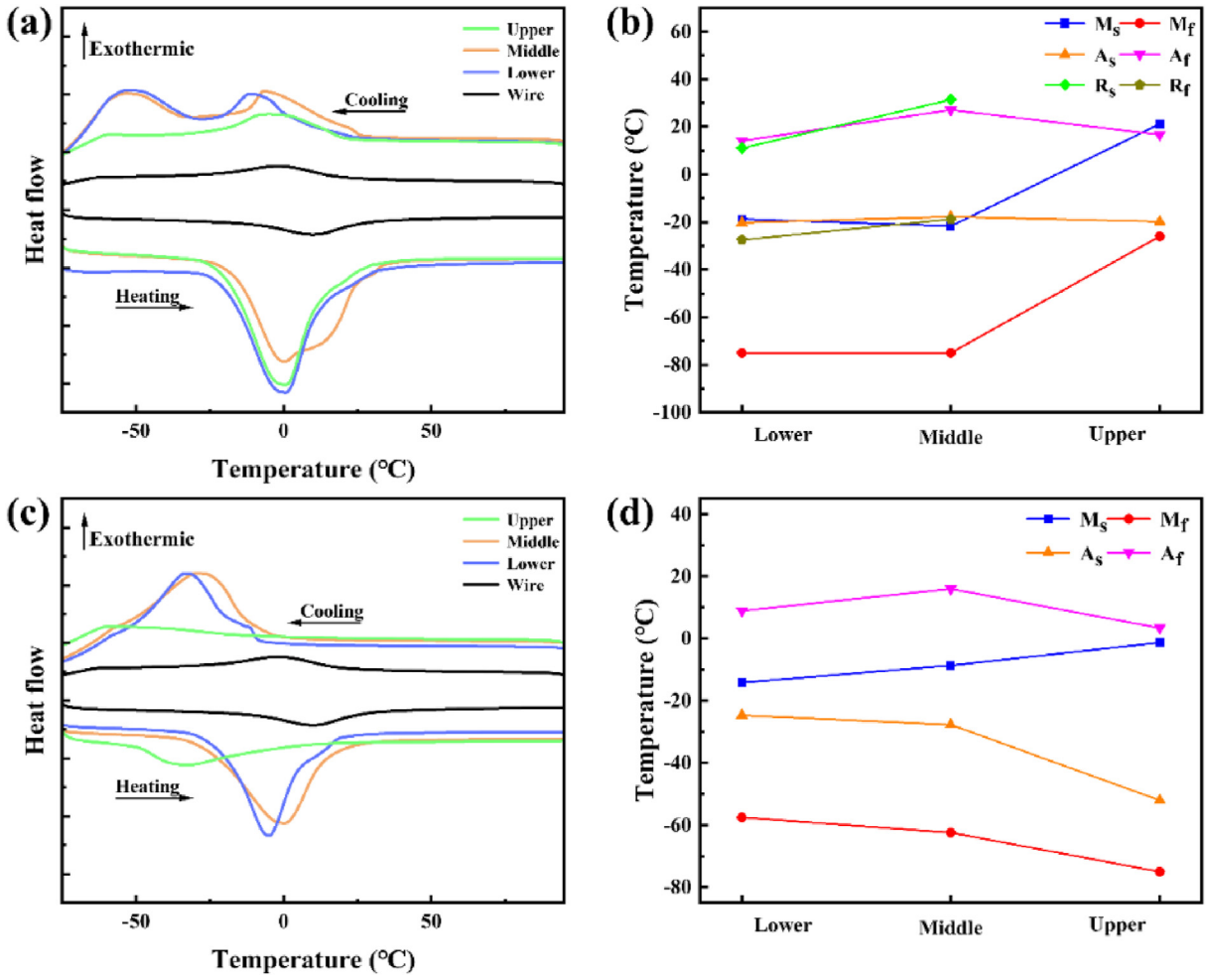

Fig. 9 – DSC results for forward and reverse martensitic phase transformation temperatures of the lower, middle, and upper regions of NiTi walls: (a)–(b) homogeneous NiTi wall; (c)–(d) heterogeneous NiTi wall.

the increase in deposition height, the upper region of the heterogeneous component with larger heat input provided higher temperatures to the generation of the precipitated phase [31]. The precipitated phase will absorb Ni atoms from the neighboring B2 matrix due to it need more Ni atoms resulting in a less Ni content in the NiTi component. For this reason, the matrix with more precipitates has a higher transition temperature.

3.6. *Tensile properties and fracture mechanism*

The results of the tensile tests in the region of different deposition heights for homogeneous NiTi walls and heterogeneous NiTi walls are shown in Fig. 10. The continuous thermal cycling behavior during the deposition of the component resulted in the formation of columnar crystals in the same direction as the deposition height [32]. The effect of WAAM deposition height and heat input on the tensile properties of NiTi alloys was investigated of horizontal direction. The yield strengths of the lower, middle and upper regions of the homogeneous components were 377.48 MPa, 344.23 MPa and 417.59 MPa, respectively. The ultimate strengths (UTS) were 606.87 MPa, 645.16 MPa and 654.45 MPa, respectively. The elongations (EL) were 12.72%, 13.97% and 15.38%, respectively. The UTS and EL increased with increasing wall height. Yield strength (YS) first decreased and then increased with

Table 3 – Phase transition temperatures (°C) of homogeneous NiTi samples and heterogeneous NiTi samples.

	Region	M_s	M_f	A_s	A_f	R_s	R_f
Homogenous	Lower	−18.81	−75.00	−20.36	14.11	11.00	−27.54
	Middle	−21.76	−75.00	−17.84	27.06	31.37	−18.89
	Upper	21.13	−26.06	−19.90	16.63	–	–
Heterogeneous	Lower	−14.24	−57.51	−24.71	8.91	–	–
	Middle	−8.69	−62.44	−27.77	15.93	–	–
	Upper	−1.36	−75.00	−52.04	3.33	–	–

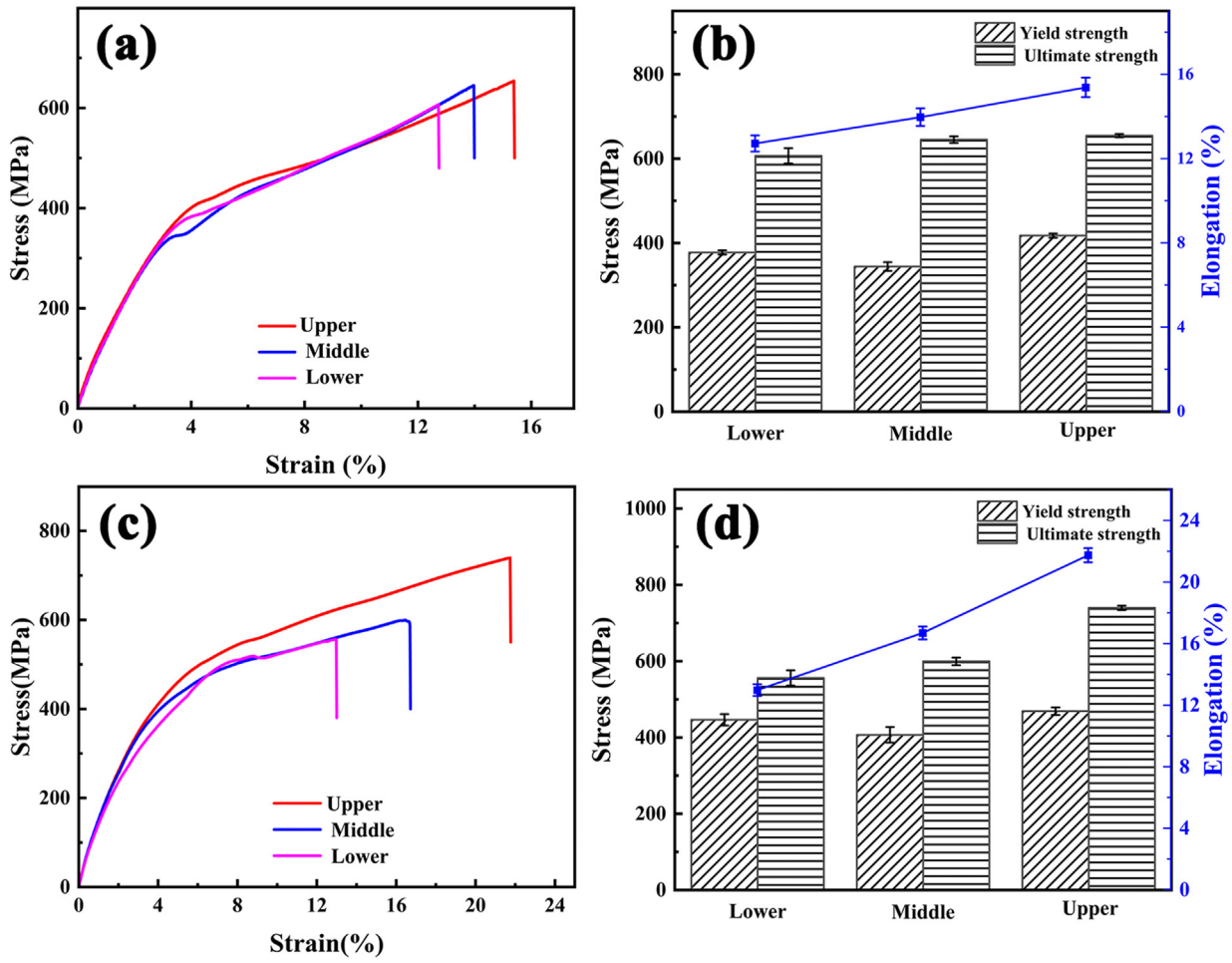

Fig. 10 – Tensile properties of the lower, middle, and upper regions of NiTi walls: (a)–(b) homogeneous NiTi wall; (c)–(d) heterogeneous NiTi wall.

increasing wall height and was highest in the upper region, as shown in Fig. 10(b). The YS of the lower, middle and upper regions of the heterogeneous NiTi alloy components were 446.4 MPa, 406.79 MPa and 468.98 MPa, respectively. The UTS were 556.12 MPa, 599.53 MPa and 739.79 MPa, respectively, and the EL were 12.98%, 16.69% and 21.74%, respectively. The YS of heterogeneous NiTi alloy components was higher than that of homogeneous NiTi alloy components at the same deposition height. The UTS of the lower and middle regions of the homogeneous NiTi alloy components were higher than that of the heterogeneous NiTi alloy components at the same deposition height, and the upper region of the heterogeneous samples have the highest UTS of 739.79 MPa. The EL of the heterogeneous NiTi alloy samples is higher than that of the homogeneous NiTi alloy samples at the same deposition height.

Firstly, Ni_4Ti_3 can strengthen the tensile properties of the sample, Ni_4Ti_3 gradually decomposed in the lower and middle regions of the matrix, resulting in a decrease in ultimate strength. Secondly, according to the Hall-Petch relation in homogeneous components, the grain size decreased with the increase of wall height, resulting in the increase of ultimate strength. With the increase of wall height, the increase of elongation was mainly due to the decrease of columnar grain size and the tendency to change to equiaxial structure. Since the heat input of the heterogeneous component is lower than that of the homogeneous component, the lower heat input will allow the heterogeneous component to cool at a higher rate, so less time will be given to the grain growth. Therefore, at the same deposition height, the elongations of heterogeneous components were higher than that of homogeneous components.

Typical fracture morphology in the tensile region for homogeneous NiTi alloy component and heterogeneous NiTi alloy component with different deposition heights is illustrated in Fig. 11 and Fig. 12. The fracture morphology of SEM fracture showed that the fracture morphology of the upper and middle regions of the tensile components of the homogeneous NiTi alloy samples can be observed to exhibit mixed tough-brittle fracture with cleavage and dimples characteristics, as shown in Fig. 11(b), (e) and (h). Significant propagation can be observed in the high magnification photographs of the three different deposition height regions of the NiTi homogeneous component as shown in Fig. 11(c), (f) and (i). In the

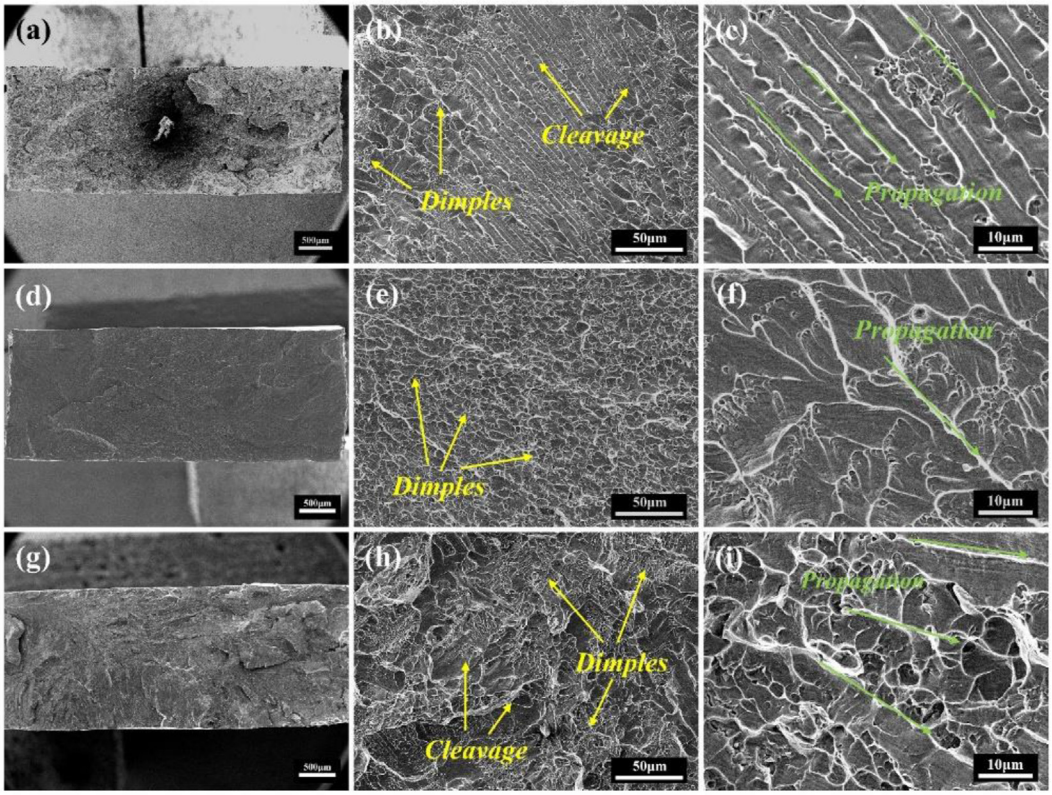

Fig. 11 – SEM images of the fracture of homogeneous NiTi tensile samples: (a)–(c) upper region; (d)–(f) middle region; (g)–(i) lower region.

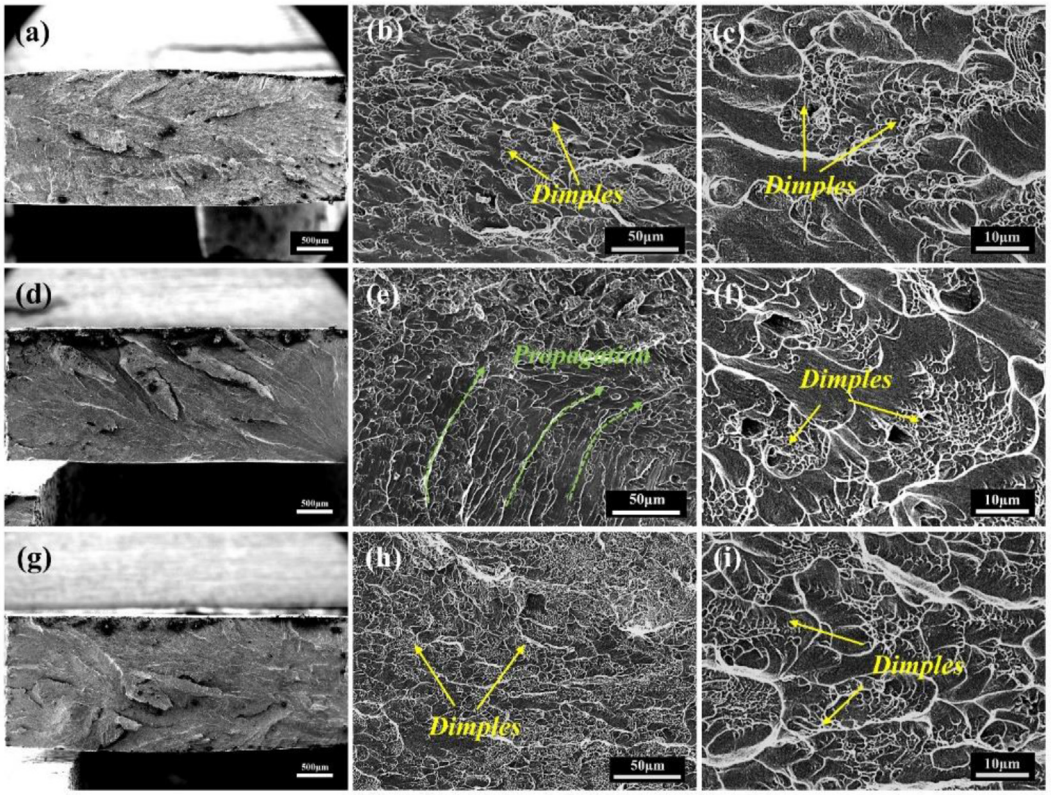

Fig. 12 – SEM images of the fracture of heterogeneous NiTi tensile samples: (a)–(c) upper region; (d)–(f) middle region; (g)–(i) lower region.

upper region, propagation characterized by parallel orientations was more intensive compared to the middle and lower regions, as shown in Fig. 11(c). In the heterogeneous NiTi alloy components, the presence of dimples on the fracture surface can be observed in the low magnification photographs of Fig. 12 (b) and (h), and parallel propagations with distinct characteristic orientations can be seen in the middle region, as illustrated in Fig. 12(e). The presence of dimples in some areas can be clearly seen from the photographs of Fig. 12 (c), (f) and (i). After the tensile test in six components, no visible cervical shrinkage deformation was found at the fracture of the component, as shown in Fig. 12(a), (d) and (g).

3.7. *Compression test and superelasticity*

The compressive properties of the different deposition height regions for the homogeneous NiTi wall and the heterogeneous NiTi wall with different deposition heights are shown in Fig. 13. From the figure, it can be seen that the stress-strain curves of all the components with homogeneous thin walls showed a "double yielding" behavior, which contained four complete phases. Elastic deformation of austenite occurred in the first stage [33,34]. When the stress reached the critical stress of stress-induced martensite phase transformation into the second stage, the austenite phase was transformed into the martensite phase. Meanwhile, the elastic deformation of martensite occurred in this stage. When the austenite phase all transformed into the martensite phase in the third stage, this time only had the elastic deformation of martensite. With the further increase of stress, the martensite phase plastic deformation transformed into the fourth stage. In the compressive fracture test, the compressive properties of each homogeneous NiTi alloy component were similar, with the compressive strength stabilized between 2500 MPa and 3000 MPa, the elongation in the range of 39%–41%, and the curves with good overlap. Among them, the middle region of homogeneous NiTi alloy component showed the best compressive strength, the compression fracture occurred at 2949.67 MPa stress and its strain of 40.69% was the largest. While the lower region of homogeneous NiTi alloy component with the weakest compressive strength experienced compression fracture at 2745.32 MPa stress. It can be seen that the stress-strain curves of all heterogeneous NiTi alloy samples were significantly dissimilar to that of homogeneous NiTi alloy samples, and there was no obvious "double yield" behavior in heterogeneous NiTi alloy samples, as illustrated in Fig. 13(b). The upper and lower curved overlap well in the compression test. In heterogeneous NiTi alloy component, the compressive strengths of the upper region and the lower region were 2534.33 MPa and 2614.16 MPa, corresponding to strains of 38.60% and 39.32%, respectively. The middle region has a superior compressive strength of 3473.43 MPa and strain of 43.94%.

Cyclic compression testing was performed for the homogeneous NiTi components and heterogeneous NiTi components in different deposition height regions, the experimental outcomes are obtained as illustrated in Fig. 14. In all samples, plastic deformation occurred during the initial stage of cyclic loading-unloading, resulting in irrecoverable strains (ε_{ir}). In the process of loading-unloading, the three different deposition height regions of the homogeneous NiTi alloy components exhibited the behavior with superelastic deformation which was illustrated in Fig. 14(a)–(c). Due to the fact that it is not possible to convert all the austenite to martensite at room temperature, the continuously loaded and unloaded NiTi samples did not recover completely after each cycle. The irrecoverable strain, recoverable strain and recovery ratio are all computed based on the curves of Fig. 14(a)–(c), and the obtained computations were exhibited at Fig. 14(d)–(f). From the calculations of the figure, it can be seen that the recoverable strains for the first cycle of the lower, middle and upper components were about 9.272%, 9.318% and 9.291%, which corresponded to recovery ratios of 92.72%, 93.18% and 92.91%. As the continuous loading and unloading process proceeds, it becomes increasingly difficult for the NiTi compression samples to recover their original length and the recovery ratios remained around 88.0%, 86.2%, and 87.6% at the 8th loading/unloading cycle. The recoverable strains for the tenth cycle of

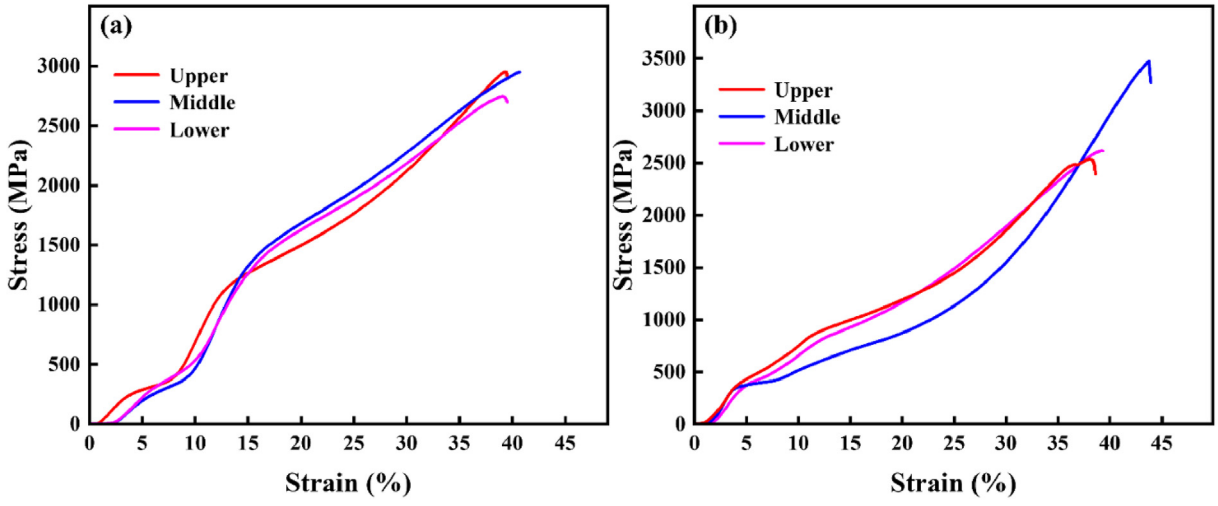

Fig. 13 – Compressive properties of the lower, middle and upper regions of the NiTi wall: (a) homogeneous NiTi wall; (b) heterogeneous NiTi wall.

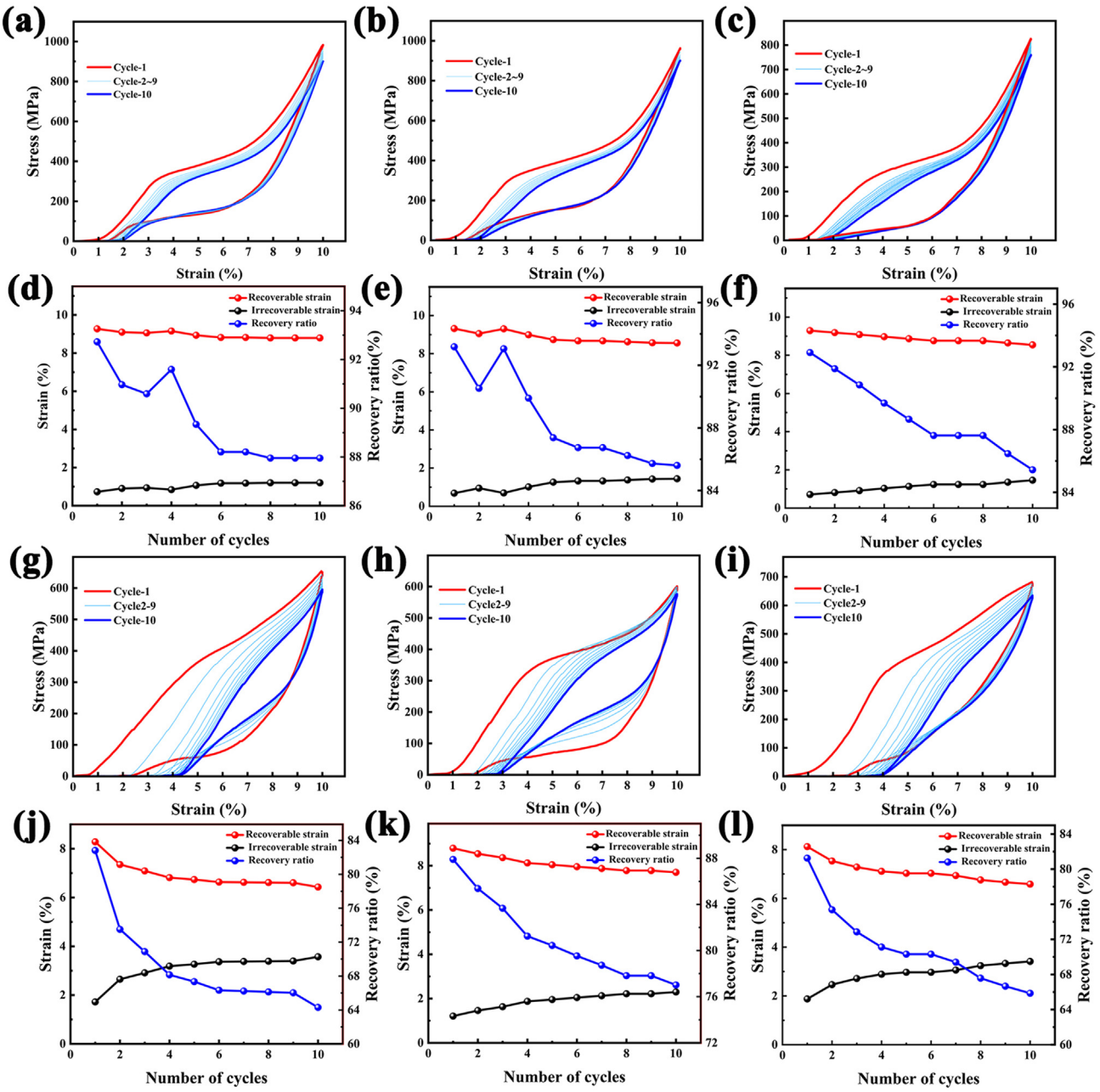

Fig. 14 – The response to load/unload cycles of lower, middle, and upper regions of NiTi walls, with the cumulative cyclic evolution of recovery ratio and irrecoverable strain. (a) and (d) lower homogenous region; (b) and (e) middle homogenous region; (c) and (f) upper homogenous region; (g) and (j) lower heterogeneous region; (h) and (k) middle heterogeneous region; (i) and (l) upper heterogeneous region.

the lower, middle and upper components were about 8.796%, 8.561% and 8.544%, corresponding to 87.96%, 85.61% and 85.44% recovery ratios. It can be seen that the difference in the deposition height of the homogeneous NiTi alloy components was not very significant for the superelasticity. The reduction of recovery ratio was due to plastic deformation during the stress-induced martensitic transformation. In addition, the accumulation of dislocations and slippage during loading process resulted in failure to recover to austenite during unloading. The phase transition interface advancement of the martensitic leaded to a reduction in stress centralization and superimposed plastic deformation, resulting in a greater change in recoverable stress. The upper, middle and lower regions of NiTi heterogeneous samples all exhibited superelastic deformation behavior during the loading-unloading process, as illustrated in Fig. 14(g)–(i). The recoverable strains for the first cycle of the upper, middle, and lower components were approximately 8.126%, 8.790%, and 8.281%, corresponding to recovery ratios of 81.26%, 87.90%, and 82.81%, as shown in Fig. 14(j)–(l). The recovery ratios decreased gradually with

the increase of the number of cycles and remained around 67.6%, 77.8%, and 66.1% at the 8th loading/unloading cycle. The recoverable strains for the tenth cycle of the upper, middle and lower components were approximately 6.586%, 7.702%, and 6.431%, corresponding to recovery ratios of 65.86%, 77.02%, and 64.31%. The compression strain of the heterogeneous NiTi alloy components was smaller and decreased faster from the first cycle to the tenth cycle compared to the homogeneous components, which showed that the homogeneous NiTi alloy samples had better superelasticity than the heterogeneous NiTi alloy samples. Moreover, according to the comparison of loading-cycling results in different regions of the heterogeneous components, the middle region samples had better superelasticity [35]. This was partly due to the fact that the columnar crystals in the middle region were finer than those in the upper and lower regions of the heterogeneous component.

The size of the columnar grains in NiTi alloys affected the superelasticity of the component [36]. In comparison, finer grain size distribution resulted in better cyclic superelasticity. The superelastic behavior of NiTi alloys was mainly related to the phase transformation between martensite and austenite, and the mutual transformation of the two phases was highly dependent on the ambient temperature of the sample. In particular, factors such as loading method, alloy composition and cycling number can also have an impact on the superelastic properties of the sample. K. Otsuka et al. [37] had studied the relationship between martensitic phase transitions and the superelasticity of NiTi alloys, where the lattice moved and rearranged during martensitic phase transitions. Atoms in the sample will move to more stable positions and release energy in this process.

There was no significant difference in superelastic properties in the building direction for the same number of loading cycles, if at a moderate (<10%) change in the rate of return. This can show that the superelastic property of the WAAM NiTi thin wall was more evenly distributed along the direction of the building. In contrast, the NiTi heterogeneous NiTi alloys prepared by WAAM exhibited microstructural nonuniformity in the build direction, which lead to different local mechanical behaviors. The middle region of the heterogeneous NiTi component has relatively fine particles and was less prone to deformation than the other two regions. As a result, more superelastic losses were observed in the upper and lower regions, hindering the complete superelastic recovery of NiTi alloys. The change in heat input had a more significant effect on the superelasticity of NiTi components prepared by WAAM than that of deposition height.

3.8. *Tribological performance*

The tribological properties of NiTi alloys are recognized to be related not only to stiffness and extensibility, at the same time to process stiffness, craze kerneling and the resistance to elongation [38]. The coefficients of friction (COF) for three different deposition height regions of WAAM homogeneous and heterogeneous NiTi walls under the same loading are compared, as shown in Fig. 15.

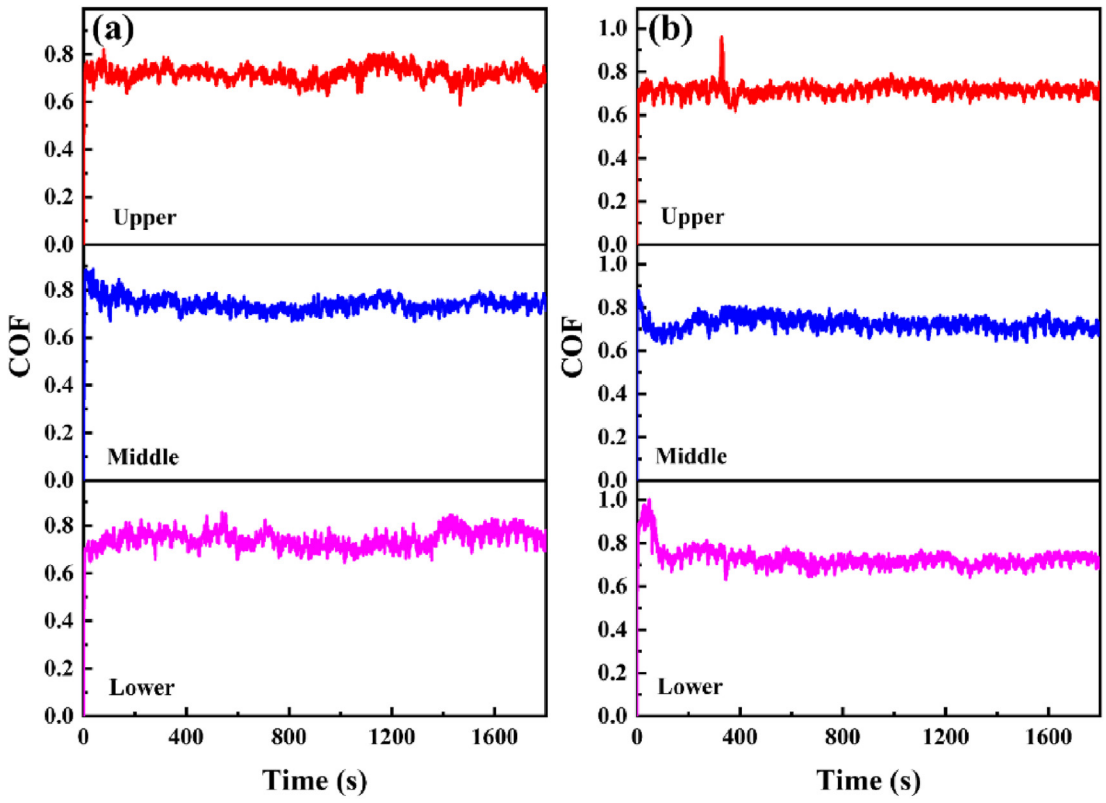

Fig. 15 – Friction coefficients of the lower, middle and upper regions of the NiTi wall: (a) homogeneous samples; (b) heterogeneous samples.

The NiTi walls produced by WAAM in this study shows no obvious cracks and pores. The microhardness and structural properties of the WAAM homogeneous NiTi alloy components shows good uniformity with increasing deposition height, resulting in moderate variations of COF in all three regions at different deposition heights. As the friction continues, the COF in all three regions of the WAAM homogeneous NiTi alloy components gradually stabilized. The COF went through a rapid upward phase and then adjusted slightly, as shown in Fig. 15(a). The COF of the upper, middle and lower regions of the WAAM homogeneous NiTi alloy samples were stabilized at about 0.715, 0.716 and 0.760, respectively. The COF of the lower region of the WAAM homogeneous NiTi component had a rising stage after 1400 s of friction. Overall, the fluctuation of the COF of the lower region of the homogeneous NiTi alloy samples was larger under the 20 N load condition, and the wear marks in the middle region of the component were stable. This may be due to the effect of deposition location, the material distribution in the middle was more uniform than the other sides. In the WAAM homogeneous NiTi alloy, compared with the remaining two regions with different deposition heights, the amplitude of the COF curves in the middle region of the component is smaller, which indicates that the wear resistance performance of the samples in this region is the most consistent among all the samples. Meanwhile, poor mechanical properties did not stably maintain material transfer during wear in the lower region, resulting in stronger COF fluctuations. In particular, in the upper region of the homogeneous NiTi component, the wear resistance was effectively improved by the existence of the B19′ phase. This was owing to the fact that the B19′ phase, as an intermediate phase, can cause a change in the stress distribution during the phase transformation process, which was able to reduce the stress concentration during the friction process. The results showed that the wear resistance of the upper region was better than that of the lower region and middle region due to the greater microhardness, superior structural properties, and larger B19′ phase content in the WAAM homogeneous NiTi component.

The COF in the middle region and lower region of the WAAM heterogeneous NiTi component decreased slightly after the rapid increase stage, and then tended to be stable with the continuous friction. After the rapid increase stage, the COF of the upper region of the heterogeneous NiTi alloy component tended to be stable as the friction continues, as shown in Fig. 15(b). The COF of the upper, middle and lower regions of the heterogeneous component was more stable than that of the homogeneous component, showing better friction stability. Compared with the COF of the three regions in the heterogeneous NiTi alloy component, the COFs of the upper, middle and lower regions were stable at 0.710, 0.720 and 0.713 respectively. The results showed that the upper region of the heterogeneous NiTi alloy sample had the best wear resistance and the friction behavior was more stable.

By analyzing the SEM morphology of wear scratches in the upper, middle and lower regions for WAAM homogeneous and heterogeneous NiTi alloy samples, the SEM results are shown in Fig. 16. The homogeneous NiTi alloy component had material buildup on both sides of the scratches in the upper, middle and lower regions, and the wear morphologies were dominated by furrows, accompanied by spalling and adhesion, as shown in Fig. 16(a)–(f). Only a small amount of oxidation appeared at the upper region of the homogeneous NiTi alloy component, as illustrated in Fig. 16(b). Moreover,

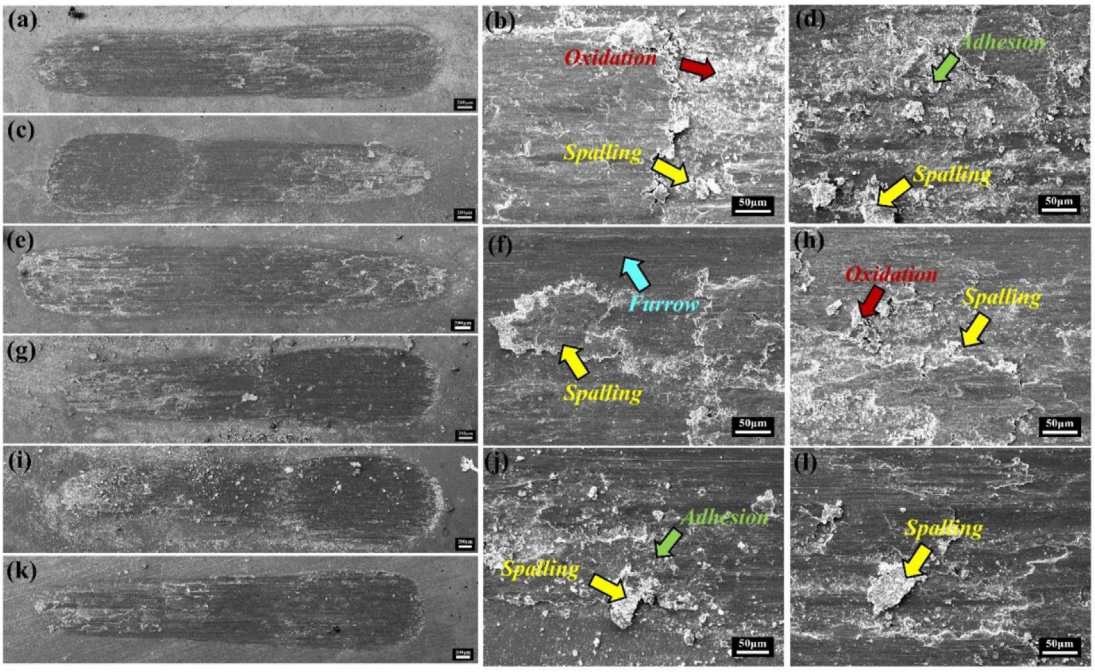

Fig. 16 – SEM macroscopic and microscopic morphology of homogeneous and heterogeneous NiTi worn surfaces: (a) and (b) homogenous upper section; (c) and (d) homogenous middle section; (e) and (f) homogenous lower section; (g) and (h) heterogeneous upper section; (i) and (j) heterogeneous middle section; (k) and (l) heterogeneous lower section.

adhesion appeared in the middle region of the homogeneous component, as shown in Fig. 16(d). The wear mechanisms of the homogeneous component were mainly oxidative wear and adhesive wear. The morphology of the wear marks on the three different deposition height regions of the heterogeneous NiTi alloy component showed a large number of furrows, with a few areas of spalling and adhesion, as shown in Fig. 16(g)–(l). Similar to homogeneous NiTi alloy component, heterogeneous NiTi alloy component also exhibited upper oxidation and middle adhesion, as shown in Fig. 16(h) and (j). This was mainly due to the lack of remelting conditions in the upper region of the component, where the cooling rate was fast, resulting in a higher oxidation content compared to the middle and lower regions [39]. The wear mechanisms of the heterogeneous NiTi alloy component were dominated by adhesive wear. The scratches of heterogeneous NiTi alloy component were more obvious than those of homogeneous component. Based on the above analysis, adhesive wear was the main form of wear mechanism in the WAAM NiTi alloy component.

4. Conclusions

In this paper, homogeneous NiTi thin wall and heterogeneous NiTi thin wall were prepared by WAAM technique. The effects of changes in deposition height and heat input on the microstructure, mechanical properties and wear behavior of NiTi alloys were investigated. The results are summarized as follows.

(1) In the homogeneous NiTi alloy samples, the columnar grains were gradually refined with the increase of deposition height. In the heterogeneous NiTi alloy samples, the lower grains were the coarsest and the middle grains were the finest. The homogeneous NiTi alloy samples mainly consisted of the B2 austenite phase, Ni_4Ti_3 phase and a small amount of $NiTi_2$ phase, while the homogeneous NiTi alloy samples mainly consisted of the B2 austenite phase and $NiTi_2$ phase.

(2) The microhardness of homogeneous NiTi alloy sample with higher heat input was higher than that of heterogeneous NiTi alloy sample for the same deposition height. The ultimate tensile strength increased from 606.87 MPa to 654.45 MPa and the elongation increased from 12.72% to 15.38% with the increase in deposition height of the homogeneous NiTi alloy samples. As the deposition height of the heterogeneous NiTi alloy samples increased, the ultimate tensile strength increased from 556.12 MPa to 739.79 MPa and the elongation increased from 12.98% to 21.74%. The yield strength and elongation of the heterogeneous NiTi alloy samples were higher than those of the homogeneous NiTi alloy samples at the same deposition height.

(3) Among the homogeneous NiTi alloy samples, the middle component had the best compressive strength, with the maximum compressive strength and corresponding compressive strain of 2949.67 MPa and 40.69%, respectively. The heterogeneous middle NiTi alloy sample showed the best compressive strength, with a maximum compressive strength and corresponding compressive strain of 3473.43 MPa and 43.94%, respectively. The recoverable strains of the lower, middle and upper samples of the homogeneous NiTi alloy were 8.796%, 8.561% and 8.544% at the tenth cycle, respectively. The cyclic compression performance becomes better as the deposition height increases. The recoverable strains of the upper, middle and lower samples of the heterogeneous NiTi alloy were 6.586%, 7.702% and 6.431% at the tenth cycle, respectively.

(4) The friction coefficients of the upper, middle, and lower regions of the homogeneous NiTi alloy samples stabilized at 0.715, 0.716 and 0.760, respectively, with the increase of the deposition height. The friction coefficients of the upper, middle, and lower regions of the heterogeneous NiTi alloy samples stabilized at 0.710, 0.720 and 0.713, respectively. The wear mechanisms of homogeneous NiTi alloy samples were mainly adhesive wear and oxidative wear. The wear mechanism of heterogeneous NiTi alloy samples was dominated by adhesive wear.

Data availability

The raw/processed data required to reproduce these findings cannot be shared at this time as the data also forms part of an ongoing study.

CRediT authorship contribution statement

J. Z. Teng: Conceptualization, Methodology, Investigation, Writing - original draft, Formal analysis, Data curation. **P. F. Jiang**: Conceptualization, Methodology, Investigation, Writing - original draft, Formal analysis, Data curation. **X. H. Cui**: Investigation. **M. H. Nie**: Data curation. **X. R. Li**: Supervision. **C. Z. Liu**: Formal analysis. **Z. H. Zhang**: Validation, Funding acquisition.

Declaration of competing interest

The authors declare that they have no known competing financial interests or personal relationships that could have appeared to influence the work reported in this paper.

Acknowledgements

This work is supported by the National Key Research and Development Program of China (Grant 2022YFB4600500) and the National Natural Science Foundation of China (Grant 52235006 and 52025053).

REFERENCES

[1] Elahinia M, Moghaddam NS, Andani MT, Amerinatanzi A, Bimber B, Hamilton R. Fabrication of NiTi through additive manufacturing: a review. Prog Mater Sci 2016;83:630–63.

[2] Liu GF, Zhou SH, Lin PY, Zong XM, Chen ZK, Zhang ZH, et al. Analysis of microstructure, mechanical properties, and wear performance of NiTi alloy fabricated by cold metal transfer based wire arc additive manufacturing. J Mater Res Technol 2022;20:246–59.
[3] Khademzadeh S. Precision additive manufacturing of NiTi shape memory parts using micro-laser powder bed fusion. Progress in Additive Manufacturing 2022;7(2):419–32.
[4] Singh S, Jinoop AN, Palani IA, Paul CP, Tomar KP, Prashanth KG. Microstructure and mechanical properties of NiTi-SS bimetallic structures built using Wire Arc Additive Manufacturing. Mater Lett 2021;303:130499.
[5] Yu L, Chen K, Zhang Y, Liu J, Yang L, Shi Y. Microstructures and mechanical properties of NiTi shape memory alloys fabricated by wire arc additive manufacturing. J Alloys Compd 2022;892:162193.
[6] Chen L, He Y, Yang Y, Niu S, Ren H. The research status and development trend of additive manufacturing technology. Int J Adv Manuf Technol 2017;89(9–12):3651–60.
[7] Li B, Wang L, Wang B, Li DH, Cui R, Su BX, et al. Solidification characterization and its correlation with the mechanical properties and functional response of NiTi shape memory alloy manufactured by electron beam freeform fabrication. Addit Manuf 2021;48:102468.
[8] Ke WC, Oliveira JP, Cong BQ, Ao SS, Qi ZW, Peng B, et al. Multi-layer deposition mechanism in ultra high-frequency pulsed wire arc additive manufacturing (WAAM) of NiTi shape memory alloys. Addit Manuf 2022;50:102513.
[9] Jiang PF, Li XR, Zong XM, Wang XB, Chen ZK, Yang HX, et al. Multi-wire arc additive manufacturing of Ti basic heterogeneous alloy: effect of deposition current on the microstructure, mechanical property and corrosion-resistance. J Alloys Compd 2022;920:166056.
[10] Jiang PF, Nie MH, Teng JZ, Liu CZ, Zhang ZH, et al. Multi-wire arc additive manufacturing of TC4-Nb-NiTi bionic layered heterogeneous alloy: microstructure evolution and mechanical properties. Mater Char 2023;202:113001.
[11] Jiang PF, Nie MH, Teng JZ, Wang XB, Liu CZ, Zhang ZH. Multi-wire arc additive manufacturing of TC4/Nb bionic layered heterogeneous alloy: microstructure evolution and mechanical properties. Mater Sci Eng, A 2023;874:145076.
[12] Zeng Z, Cong BQ, Oliveira JP, Ke WC, Schell N, Peng B, et al. Wire and arc additive manufacturing of a Ni-rich NiTi shape memory alloy: microstructure and mechanical properties. Addit Manuf 2020;32:101051.
[13] Zhang M, Fang X, Wang Y, Jiang X, Chang TX, Xi NY, et al. High superelasticity NiTi fabricated by cold metal transfer based wire arc additive manufacturing. Mater Sci Eng, A 2022;840:143001.
[14] Jiang PF, Nie MH, Zong XM, Wang XB, Chen ZK, Liu CZ, et al. Microstructure and mechanical properties of TC4/NiTi bionic gradient heterogeneous alloy prepared by multi-wire arc additive manufacturing. Mater Sci Eng, A 2023;866:144678.
[15] Zhao C, Liang H, Luo S, Yang J, Wang Z, et al. The effect of energy input on reaction, phase transition and shape memory effect of NiTi alloy by selective laser melting. J Alloys Compd 2020;817:153288.
[16] Resnina N, Palani IA, Belyaev S, Singh S, Liulchak P, Karaseva U, et al. Influence of heat treatment on the structure and martensitic transformation in NiTi alloy produced by wire arc additive manufacturing. Materialia 2021;20:101238.
[17] Liu S, Wan D, Peng D, Lu X, Ren X, Fu Y, et al. Effect of heat input on nanomechanical properties of wire-arc additive manufactured Al 4047 alloys. Mater Sci Eng, A 2022;860:144288.
[18] Wang J, Pan Z, Carpenter K, Han J, Wang Z, Li H. Comparative study on crystallographic orientation, precipitation, phase transformation and mechanical response of Ni-rich NiTi alloy fabricated by WAAM at elevated substrate heating temperatures. Mater Sci Eng, A 2021;800:140307.
[19] Wang J, Pan Z, Wang Y, Wang L, Su L, Cuiuri D, et al. Evolution of crystallographic orientation, precipitation, phase transformation and mechanical properties realized by enhancing deposition current for dual-wire arc additive manufactured Ni-rich NiTi alloy. Addit Manuf 2020;34:101240.
[20] Pu Z, Du D, Wang K, Liu G, Zhang D, Wang X, et al. Microstructure, phase transformation behavior and tensile superelasticity of NiTi shape memory alloys fabricated by the wire-based vacuum additive manufacturing. Mater Sci Eng 2021;812:141077.
[21] Wang Z, Palmer TA, Beese AM. Effect of processing parameters on microstructure and tensile properties of austenitic stainless steel 304L made by directed energy deposition additive manufacturing. Acta Mater 2016;110:226–35.
[22] Kelly SM, Kampe SL. Microstructural evolution in laser-deposited multilayer Ti-6AI-4V builds: Part II. Thermal modeling. Metall Mater Trans 2004;35(6):1869–79.
[23] Tang W, Shen Q, Yao X, Li W, Jiang J, Ba Z, et al. Effect of grain size on the microstructure and mechanical anisotropy of stress-induced martensitic NiTi alloys. Mater Sci Eng 2022;849:143497.
[24] Andani MT, Saedi S, Turabi AS, Karamooz MR, Haberland C, Karaca HE, et al. Mechanical and shape memory properties of porous Ni50.1Ti49.9 alloys manufactured by selective laser melting. J Mech Behav Biomed Mater 2017;68:224–31.
[25] Liu S, Lin Y, Wang G, Wang X. Effect of varisized Ni_4Ti_3 precipitate on the phase transformation behavior and functional stability of Ti-50.8at.% Ni alloys. Mater Char 2021;172:110832.
[26] Wang J, Pan Z, Yang G, Han J, Chen X, Li H. Location dependence of microstructure, phase transformation temperature and mechanical properties on Ni-rich NiTi alloy fabricated by wire arc additive manufacturing. Mater Sci Eng 2019;749:218–22.
[27] Wang W, Cheng P, Li X, Gao Y, Wang K. Effects of nickel content on mechanical and tribological properties of NiTi alloy. Rare Met Mater Eng 2021;50(12):4418–28.
[28] Xia M, Liu P, Sun Q. Grain size dependence of Young's modulus and hardness for nanocrystalline NiTi shape memory alloy. Mater Lett 2018;211:352–5.
[29] Han J, Chen XY, Zhang GY, Lu LZ, Xin Y, Liu B, et al. Microstructure and mechanical properties of $Ni_{50.8}Ti_{49.2}$ and $Ni_{53}Ti_{47}$ alloys prepared in situ by wire-arc additive manufacturing. J Mater Process Technol 2022;306:117631.
[30] Frenzel J, George EP, Dlouhy A, Somsen C, Wagner MF-X, Eggeler G. Influence of Ni on martensitic phase transformations in NiTi shape memory alloys. Acta Mater 2010;58(9):3444–58.
[31] Feng Y, Liu B, Wan X, Liu Q, Lin X, Wang P. Influence of processing parameter on phase transformation and superelastic recovery strain of laser solid forming NiTi alloy. J Alloys Compd 2022;908:164568.
[32] Sam J, Franco B, Ma J, Karaman I, Elwany A, Mabe JH. Tensile actuation response of additively manufactured nickel-titanium shape memory alloys. Scripta Mater 2018;146:164–8.
[33] Zhu SL, Yang XJ, Fu DH, Zhang LY, Li CY, Cui ZD. Stress-strain behavior of porous NiTi alloys prepared by powders sintering. Mater Sci Eng 2005;408(1–2):264–8.
[34] Glezer AM, Metlov LS, Sundeev RV, Shalimova AV. On the nature of the "double" yield point in $Ti_{50}Ni_{25}Cu_{25}$ alloy upon high-pressure torsion. JETP Lett 2017;105(5):332–4.

[35] Oliveira JP, Fernandes FMB, Schell N, Miranda RM. Martensite stabilization during superelastic cycling of laser welded NiTi plates. Mater Lett 2016;171:273–6.
[36] Li BY, Rong LJ, Li YY. Microstructure and superelasticity of porous NiTi alloy. Sci China E 1999;42(1):94–9.
[37] Otsuka K, Ren X. Physical metallurgy of Ti-Ni-based shape memory alloys. Prog Mater Sci 2005;50(5):511–678.
[38] Yu Z, Xu Z, Guo Y, Sha P, Liu R, Xin R, et al. Analysis of microstructure, mechanical properties, wear characteristics and corrosion behavior of SLM-NiTi under different process parameters. J Manuf Process 2022;75:637–50.
[39] Lin PY, Zhu YF, Zhou H, Wang CT, Ren LQ. Wear resistance of a bearing steel processed by laser surface remelting cooled by water. Scripta Mater 2010;63(8):839–42.